

## Mechanism of Enantioselective C–C Bond Formation with Bifunctional Chiral Ru Catalysts: NMR and DFT Study

Ilya D. Gridnev, Masahito Watanabe, Hui Wang, and Takao Ikariya\*

Department of Applied Chemistry, Graduate School of Science and Engineering, Tokyo Institute of Technology, O-okayama, Meguro-ku, Tokyo 152-8552, Japan

Received August 23, 2010; E-mail: tikariya@apc.titech.ac.jp

**Abstract:** The mechanism of Michael addition reactions of 1,3-dicarbonyl compounds to cyclic enones catalyzed by bifunctional Ru catalysts bearing N-sulfonylated (*R,R*)-DPEN ligands (DPEN = (*R,R*)-1,2-diphenylethylenediamine) was studied by NMR and DFT computational analyses. NMR investigation of the stoichiometric reactions of chiral amido Ru complexes, Ru(N-sulfonylated dpen)( $\eta^6$ -arene) **1a–c**, with dimethyl malonate **2** and  $\beta$ -keto ester **3** revealed that at decreased temperatures deprotonation proceeds in a stereoselective manner to provide amine complexes. The reaction with malonic ester **2** provided exclusively C-bound amino Ru complexes **6a,c**, while the reaction of  $\beta$ -keto ester **3** gave an equilibrium mixture of rapidly interconverting C- and O-bound complexes. The structures of C-bound Ru complex **6c** and O-bound Ru complex **9c** were determined by single crystal X-ray analysis. A computational study showed that the enantioselective C–C bond formation proceeds through intermediate formation of chelating ion pairs that coordinate a molecule of enone via the Ru metal center producing a highly organized environment for the C–C bond formation, yielding selectively only one enantiomer of the product. Systematic study of a series of the catalyst–substrate combinations revealed that the experimentally observed sense of enantioselection was consistently explained by computational analysis. The tendency of increasing ee with the bulk of the coordinated arene in Ru complex is reproduced computationally by changes in the difference of either ZPPE-corrected energies or Gibbs free energies for *S*- and *R*-pathways.

### 1. Introduction

Recent rapid progress in the design of chiral bifunctional molecular catalysts with an acid–base synergy effect enables the development of highly efficient molecular transformations for organic synthesis.<sup>1</sup> Many conceptually new metal-based bifunctional catalyst systems have been reported, which contain two or more active sites for the activation of electrophiles and nucleophiles to facilitate a wide range of catalytic enantioselective reactions. The reacting substrates can be efficiently bound and activated in a concerted manner on the neighboring active centers in the same molecule. Although these molecular catalysts promote asymmetric molecular transformations, their specific structural features often make them suffer from the acid–base neutralization, leading to the deactivation of the catalysts. Therefore, precise spatial organization of the functionality in the catalyst molecule is required to achieve the best catalytic performance.<sup>2,3</sup>

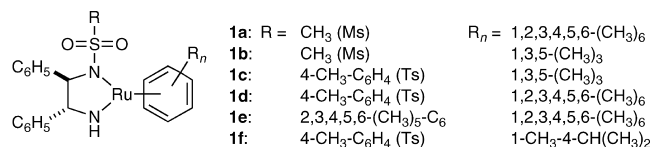
We have successfully developed chiral bifunctional molecular catalysts bearing chiral N-sulfonylated 1,2-diamine ligands, Ru[(*R,R*)-Tsdpen]( $\eta^6$ -arene) (**1**) ((*R,R*)-TsDPEN: (*R,R*)-*N*-(*p*-

toluenesulfonyl)-1,2-diphenylethylenediamine), for asymmetric transfer hydrogenation of ketones and imines. Chiral bifunctional amido Ru complexes **1** are the catalysts, and chiral amine hydrido metal complexes exhibiting a metal/NH synergetic effect are involved in the catalytic cycle as intermediates.<sup>2,4</sup> The amino complexes are capable of binding substrates via two active sites in the same molecule. This feature is important for enantioselective transformations, since it dramatically restricts the number of productive substrate orientations during the coordination. Accordingly, quite a few highly enantioselective reductions utilizing these bifunctional catalysts have been developed.<sup>4</sup>

- (3) (a) Haack, K.-J.; Hashiguchi, S.; Fujii, A.; Ikariya, T.; Noyori, R. *Angew. Chem., Int. Ed. Engl.* **1997**, *36*, 285. (b) Casey, C. P.; Singer, S. W.; Powell, D. R.; Hayashi, R. K.; Lavana, M. *J. Am. Chem. Soc.* **2001**, *123*, 1090. (c) Abdur-Rashid, K.; Clapham, S. E.; Hadzovic, A.; Harvey, J. N.; Lough, A. J.; Morris, R. H. *J. Am. Chem. Soc.* **2002**, *124*, 15104. (d) Casey, C. P.; Johnson, J. B. *J. Org. Chem.* **2003**, *68*, 1998. (e) Sandoval, C. A.; Ohkuma, T.; Muniz, K.; Noyori, R. *J. Am. Chem. Soc.* **2003**, *125*, 13490. (f) Johnson, J. B.; Bäckvall, J.-E. *J. Org. Chem.* **2003**, *68*, 1998. Clapham, S. E.; Hadzovic, A.; Morris, R. H. *Coord. Chem. Rev.* **2004**, *248*, 2201. (g) Zhang, J.; Gandelman, M.; Shimon, L. J. W.; Rozenberg, H.; Milstein, D. *Organometallics* **2004**, *23*, 4026. (h) Zhang, J.; Leitus, G.; Ben-David, Y.; Milstein, D. *J. Am. Chem. Soc.* **2005**, *127*, 10840. (i) Kohl, S.; Weiner, L.; Schwartsburd, L.; Konstantinovski, L.; Shimon, L. J. W.; Ben-David, Y.; Iron, M.; Milstein, D. *Science* **2009**, *324*, 74. (j) Samec, J. S. M.; Bäckvall, J.-E.; Andersson, P. G.; Brandt, P. *Chem. Soc. Rev.* **2006**, *35*, 237. (k) Zweifel, T.; Naubron, J.-V.; Büttner, T.; Ott, T.; Grützmacher, H. *Angew. Chem., Int. Ed.* **2008**, *47*, 3245. (l) Hamilton, R. J.; Bergens, S. H. *J. Am. Chem. Soc.* **2008**, *130*, 11979. (m) Läng, F.; Breher, F.; Stein, D.; Grützmacher, H. *Organometallics* **2005**, *24*, 2997. (n) Zweifel, T.; Naubron, J.-V.; Grützmacher, H. *Angew. Chem., Int. Ed.* **2008**, *48*, 559.

- (1) (a) Noyori, R. *Asymmetric Catalysis in Organic Synthesis*; Wiley: New York, 1994. (b) Ojima, I. *Catalytic Asymmetric Synthesis*, 2nd ed.; Wiley: New York, 2000. (c) Jacobsen, E. N.; Pfaltz, A.; Yamamoto, H. *Comprehensive Asymmetric Catalysis*; Springer: Heidelberg, Germany, 1999. (d) Walsh, P. J.; Kozlowski, M. C. *Fundamentals in Asymmetric Catalysis*; USB: Sausalito, CA, 2008.
- (2) (a) Noyori, R.; Hashiguchi, S. *Acc. Chem. Res.* **1997**, *30*, 97. (b) Ikariya, T.; Blacker, A. J. *Acc. Chem. Res.* **2007**, *40*, 1300. (c) Ikariya, T.; Murata, K.; Noyori, R. *Org. Biomol. Chem.* **2006**, *4*, 393–406. (d) Ikariya, T.; Gridnev, I. D. *Chem. Rec.* **2009**, *9*, 106.

chiral amido Ru cat:



The mechanistic aspects of enantioselective reduction with bifunctional catalysts are intensively studied experimentally and computationally.<sup>2,4</sup> It is commonly accepted that hydrogen transfer between ketones and alcohols occurs through a six-membered pericyclic transition state, in which the substrate can be activated in a concerted manner as shown in Figure 1.

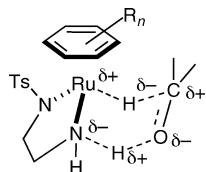
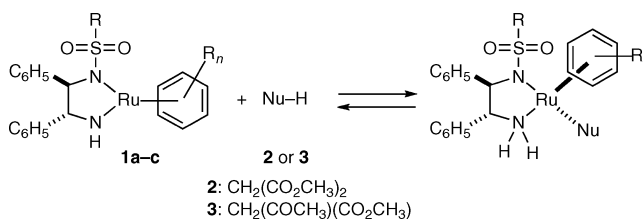


**Figure 1.** A possible transition state for the hydrogen transfer between ketones and alcohols.

There are several important implications of this mechanism. First, it demonstrates that the double bond of the prochiral carbonyl compound is fixed by two binding sites of the catalyst in a dual activation mode, thus opening the door for effective stereodiscrimination. Next, since the metal center of the bifunctional catalyst shown in Figure 1 has a coordinatively saturated environment, the reacting substrate does not interact directly with the metal center, thus its activation with the catalyst takes place in the outer sphere. This kind of transition structure results in the complete reversibility of the reaction which is practically important, since the same catalytic systems can be used either for enantioselective reduction of ketones or for kinetic resolution of alcohols via selective oxidation, as well as for rapid racemization of chiral alcohols with an achiral bifunctional catalyst system.<sup>4f,5</sup>

On the other hand, the enantioselective C–C bond formation with bifunctional molecular catalysts has been much less studied. The known examples are Shibasaki's chiral multimetallic centered catalysts,<sup>6</sup> Ito and Hayashi's chiral gold catalysts,<sup>7a</sup> Mezzetti's ruthenium PNNP complexes,<sup>8</sup> and Ru hydride borohydride complexes of Morris.<sup>9</sup> We have recently found that chiral amido complexes have a sufficient Brønsted basicity to effect deprotonation of certain acidic pronucleophiles, leading to the corresponding amino complex that binds the deprotonated nucleophile as shown in Scheme 1.<sup>10</sup> Hence, formally the situation resembles the case of asymmetric transfer hydrogenation (Figure 1), the metal atom being bonded to the correspond-

### Scheme 1. Reactions of Chiral Amido Complexes with Pronucleophiles



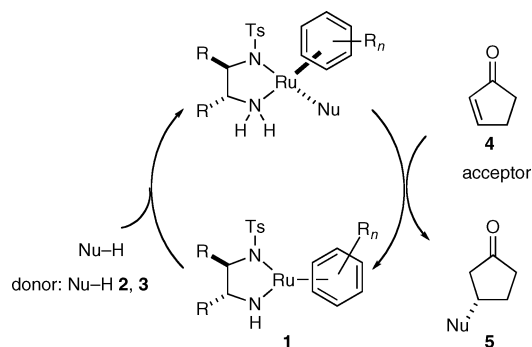
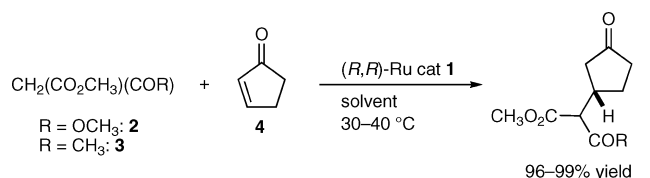
ing organic moiety instead of the hydrogen atom. This similarity initially led to the conclusion that the reaction with a second player in the C–C bond formation reaction might proceed via an analogous transition structure, i.e. direct transfer of the metal bonded nucleophilic part to the acceptor assisted by coordination of the latter to the NH<sub>2</sub> group of the amino complex. In fact, we found that the chiral Ru catalysts, Ru(N-sulfonylated dpen)(η<sup>6</sup>-arene) **1**, efficiently effected enantioselective Michael addition of 1,3-dicarbonyls to cyclic enones or nitroalkenes to give the corresponding chiral adducts with excellent ee's.<sup>11</sup>

There also are distinctions between the structures of amino complexes having a hydrogen atom or an organic moiety bonded to the metal. In the former case, the electronic density acquired by the proton upon the formation of the M–H bond is localized on the hydride ligand. Whereas when a conjugated organic moiety binds to the metal, the charge can be effectively delocalized, and the reactive center can be shifted to another part of the molecule. Also, replacing the hydrogen atom with any organic moiety dramatically increases the spatial hindrance nearby the metal atom which can evidently prevent the formation of a transition state similar to the hydrogen transfer case.

In this paper we report an experimental mechanistic study on these types of C–C bond formation reactions with bifunctional catalysts, combined with a computational investigation of the catalytic cycle and the origin of enantioselectivity. Scheme 2 illustrates a schematic catalytic cycle for the enantioselective

- (4) (a) Hashiguchi, S.; Fujii, A.; Takehara, J.; Ikariya, T.; Noyori, R. *J. Am. Chem. Soc.* **1995**, *117*, 7562. (b) Takehara, J.; Hashiguchi, S.; Fujii, A.; Inoue, S.; Ikariya, T.; Noyori, R. *Chem. Commun.* **1996**, 233. (c) Gao, J.-X.; Ikariya, T.; Noyori, R. *Organometallics* **1996**, *15*, 1087. (d) Fujii, A.; Hashiguchi, S.; Uematsu, N.; Ikariya, T.; Noyori, R. *J. Am. Chem. Soc.* **1996**, *118*, 2521. (e) Uematsu, N.; Fujii, A.; Hashiguchi, S.; Ikariya, T.; Noyori, R. *J. Am. Chem. Soc.* **1996**, *118*, 4916. (f) Hashiguchi, S.; Fujii, A.; Haack, K.-J.; Matsumura, T.; Ikariya, T.; Noyori, R. *Angew. Chem., Int. Ed. Engl.* **1997**, *36*, 288. (g) Matsumura, K.; Hashiguchi, S.; Ikariya, T.; Noyori, R. *J. Am. Chem. Soc.* **1997**, *119*, 8738. (h) Ikariya, T.; Hashiguchi, S.; Murata, K.; Noyori, R. *Org. Synth.* **2005**, *82*, 10.
- (5) (a) Arita, S.; Koike, T.; Kayaki, Y.; Ikariya, T. *Angew. Chem., Int. Ed.* **2008**, *47*, 2447. (b) Ito, M.; Osaku, A.; Kitahara, S.; Hirakawa, M.; Ikariya, T. *Tetrahedron Lett.* **2003**, *44*, 7521.

- (6) (a) Shibasaki, M.; Sasai, H.; Arai, T. *Angew. Chem., Int. Ed. Engl.* **1997**, *36*, 1236. (b) Shibasaki, M.; Kanai, M.; Funahashi, K. *Chem. Commun.* **2002**, 1989. (c) Shibasaki, M.; Yoshikawa, Y. *Chem. Rev.* **2002**, *102*, 2187. (d) Oisaki, K.; Zhao, D.; Kanai, M.; Shibasaki, M. *J. Am. Chem. Soc.* **2007**, *129*, 7439. (e) Shibasaki, M.; Matsunaga, S.; Kumagai, N. *Synlett* **2008**, 1583. Nitabar, T.; Nojiri, A.; Kobayashi, M.; Kumagai, N.; Shibasaki, M. *J. Am. Chem. Soc.* **2009**, *131*, 13860. (f) Mashiko, T.; Kumagai, N.; Shibasaki, M. *J. Am. Chem. Soc.* **2009**, *131*, 14990. (g) Shibasaki, M.; Kanai, M.; Matsunaga, S.; Kumagai, N. *Acc. Chem. Res.* **2009**, *42*, 1117.
- (7) Early review articles for enantioselective C–C bond formation with bifunctional catalysts: (a) Sawamura, M.; Ito, Y. *Chem. Rev.* **1992**, *92*, 857. (b) Steinhagen, H.; Helmchen, G. *Angew. Chem., Int. Ed. Engl.* **1996**, *35*, 2339. (c) van den Beuken, E. K.; Feringa, B. L. *Tetrahedron* **1998**, *54*, 12985. (d) Rowlands, G. J. *Tetrahedron* **2001**, *57*, 1865. (e) Gröger, H. *Chem.—Eur. J.* **2001**, *7*, 5246. (f) Ma, J.-A.; Cahard, D. *Angew. Chem., Int. Ed.* **2004**, *43*, 4566.
- (8) (a) Althaus, M.; Bonnacorsi, C.; Mezzetti, A.; Santoro, F. *Organometallics* **2006**, *25*, 3108. (b) Santoro, F.; Althaus, M.; Bonnacorsi, C.; Gischig, S.; Mezzetti, A. *Organometallics* **2008**, *27*, 3866. (c) Schotes, C.; Mezzetti, A. *J. Am. Chem. Soc.* **2010**, *132*, 3652.
- (9) (a) Guo, R.; Morris, R. H.; Song, D. *J. Am. Chem. Soc.* **2005**, *127*, 516. (b) Clapham, S. E.; Guo, R.; Zimmer-De Iulius, M.; Rasool, N.; Lough, A.; Morris, R. H. *Organometallics* **2006**, *25*, 5477.
- (10) (a) Murata, K.; Konishi, H.; Ito, M.; Ikariya, T. *Organometallics* **2002**, *21*, 253. (b) Koike, T.; Ikariya, T. *Adv. Synth. Catal.* **2004**, *346*, 37. (c) Koike, T.; Ikariya, T. *Organometallics* **2005**, *24*, 724.
- (11) (a) Watanabe, M.; Murata, K.; Ikariya, T. *J. Am. Chem. Soc.* **2003**, *125*, 7509. (b) Wang, H.; Watanabe, M.; Ikariya, T. *Tetrahedron Lett.* **2005**, *46*, 963. (c) Watanabe, M.; Ikaigawa, H.; Wang, H.; Murata, K.; Ikariya, T. *J. Am. Chem. Soc.* **2004**, *126*, 11148. (d) Ikariya, T.; Wang, H.; Watanabe, M.; Murata, K. *J. Organomet. Chem.* **2004**, *689*, 1377.

**Scheme 2.** A Schematic Catalytic Cycle for Enantioselective Michael Addition with Chiral Catalyst **1****Scheme 3.** Enantioselective Michael Reactions with Chiral Amido Ru Complexes

donor	acceptor	Ru cat	solvent	ee, %
<b>2</b>	<b>4</b>	<b>1a</b>	(CH <sub>3</sub> ) <sub>3</sub> COH	98
<b>2</b>	<b>4</b>	<b>1c</b>	(CH <sub>3</sub> ) <sub>3</sub> COH	89
<b>2</b>	<b>4</b>	<b>1d</b>	(CH <sub>3</sub> ) <sub>3</sub> COH	98
<b>3</b>	<b>4</b>	<b>1a</b>	toluene	85
<b>3</b>	<b>4</b>	<b>1c</b>	toluene	90
<b>3</b>	<b>4</b>	<b>1d</b>	toluene	91

The molar ratio of donor:acceptor:Ru is 50:50–60:1.

C–C bond formation with the bifunctional chiral amido Ru catalyst. The presence of an NH moiety in the cooperating ligands is crucially important for the catalytic performance.

## 2. Results and Discussion

**2.1. Reactions under Study.** The chiral bifunctional amido Ru complexes bearing a chiral TsDPEN ligand catalyze enantioselective Michael reactions of cyclic  $\alpha,\beta$ -unsaturated ketones with malonates **2** and  $\beta$ -keto esters **3** to the corresponding adducts with excellent yields and ee's. The representative results are listed in Scheme 3.<sup>11a,b</sup> For example, a reaction of dimethyl malonate **2** and cyclopentenone **4** in a 1:1 molar ratio in *tert*-butyl alcohol containing the (*R,R*)-chiral amido Ru complex at 40 °C gives the corresponding (*S*)-Michael adduct in an almost

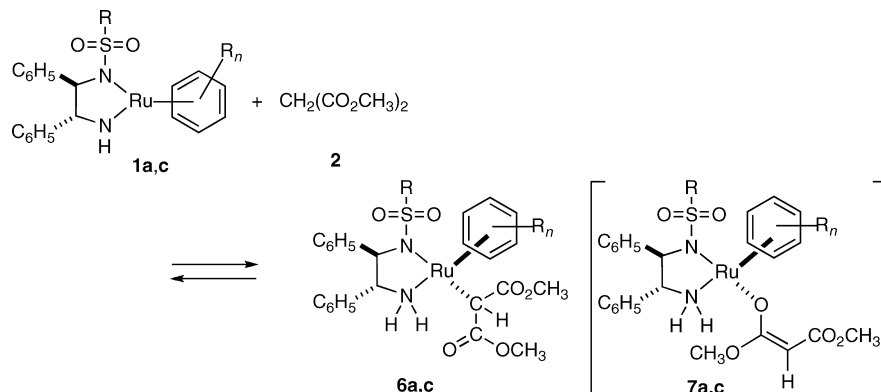
quantitative yield and with an excellent ee. When  $\beta$ -keto esters **3** were used as the Michael donor, the reaction was quantitative, providing chiral adducts with excellent ee at the stereogenic carbon atom on the cyclopentanone, although as a 1:1 mixture of diastereomers with both absolute configurations at the donor carbon. The stereochemical outcome of the reaction was delicately influenced by the structures of the diamine and arene ligands as well as the donor and acceptors. *tert*-Butyl alcohol, toluene, and THF can be used as practical solvents, while CH<sub>2</sub>Cl<sub>2</sub> gives a reasonably high ee albeit a slightly lower activity.<sup>11a,b</sup> As can be seen from Scheme 3, the MsDPEN complex **1a** or TsDPEN complex **1d** gave the chiral adducts with high ee's. The fine-tuning of the chiral amido catalyst is required in each case to achieve the utmost efficiency. Thus, in the case of the Michael additions to  $\alpha,\beta$ -unsaturated ketones, the catalysts **1a,d** that have hexamethylbenzene as the coordinated arene ligand provided the best ee, whereas the catalysts with less crowded arenes gave inferior results (see also Table 5).<sup>11</sup>

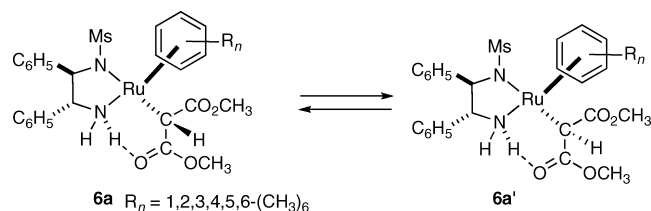
**2.2. Experimental Studies of the Reactions of Chiral Amido Complexes with Nucleophiles.** **2.2.1. Reactions of Ru Complexes **1a** and **1c** with Dimethyl Malonate **2**.** We have experimentally investigated intermediates in the reactions catalyzed by complexes **1a** and **1c**. The former gave the best results from the point of view of enantioselection, and the X-ray data of complex **1c** and its related complexes are available. The catalyst **1b** and all intermediates derived from it have been used as the starting point for the computational study because of their relatively small size.

Addition of an excessive amount of dimethyl malonate **2** to a CD<sub>2</sub>Cl<sub>2</sub> solution of complex **1a** or **1c** led to the formation of the corresponding C-bound complexes **6a** or **6c** (Scheme 4).<sup>12,13</sup> Formation of the corresponding O-bound complexes **7a** or **7c** could not be detected.

The most characteristic features in the NMR spectra of **6a** identifying it as the C-bound complex are the signals of the Ru bonded CH unit. The carbon atom bound to Ru resonates at  $\delta$  27.04, whereas the corresponding proton exhibits a broad singlet at  $\delta$  3.95 that is correlated to both of the nonequivalent carbonyls ( $\delta = 176.16, 181.84$ ) in the HMBC spectrum at  $-50^\circ\text{C}$ .

Variable temperature NMR study of complex **6a** showed that there are three dynamic processes for this complex in various temperature intervals. Two species in a 1:3 ratio with very similar <sup>1</sup>H and <sup>13</sup>C NMR spectra were observed at  $-90^\circ\text{C}$ . The chemical exchange between these two species is very fast resulting in averaging of their signals already at  $-50^\circ\text{C}$  to give cleanly one set of signals corresponding to **6a**. Since in both

**Scheme 4.** Stoichiometric Reactions of Chiral Amido Complexes **1** with Dimethyl Malonate **2**

Scheme 5. Possible Structures of C-Bound Complex **6a** in Solution

observed species one of the NH protons is H-bound ( $\delta = 6.35$  (major) and 6.48 (minor)), most probably these line shape changes are due to the exchange between two complexes with alternatively H-bound carboxymethyl groups which are non-equivalent due to the proximity of the chiral Ru atom center (Scheme 5).

The phase-sensitive  $^1\text{H}$ - $^1\text{H}$  NOESY spectrum at  $-50\text{ }^\circ\text{C}$  (Figure 2) revealed a pairwise exchange between nonequivalent ortho- and meta-protons of the phenyl group adjacent to the N-Ms moiety of **6a**. This observation testifies to the hindered rotation of this phenyl ring that is trapped between another phenyl and the Ms group that must keep a definite conformation to avoid the encounter with the hexamethylbenzene ring which demonstrates significant steric hindrance in the molecule of the C-bound complex **6a**. Moreover, the low-field ortho-proton ( $\delta = 7.46$ ) has a strong NOE with the methyl groups of the coordinated arene that proves an *S* configuration around the Ru atom in **6a**.

The third dynamic process observed for **6a** is its equilibrium with amido complex **1a** and free substrate **2**. This process begins to affect the line shape in the  $^1\text{H}$  and  $^{13}\text{C}$  NMR spectra at  $-20\text{ }^\circ\text{C}$  and is, therefore, slower than the two processes described above.

Very similar observations were made for complex **6c**. In this case it was possible to determine the solid state structure of **6c** by single-crystal X-ray analysis (Table 1 and Figure 3). Similarly to **6a**, the complex **6c** has an *S*-configuration around the Ru atom. Noteworthy is the significant deviation from the ideal piano-stool geometry in the value of the angle made by the Ru-C bond and the plane of the coordinated arene (Table 1). Apparently, this deviation reflects the steric hindrance that is encountered by the substituents in a C-bound complex.

**2.2.2. Reactions of Ru Complexes 1a and 1c with  $\beta$ -Keto Ester 3.** Addition of 1.5 equiv of  $\beta$ -keto ester **3** to a  $\text{CD}_2\text{Cl}_2$  solution of Ru complex **1a** led to deprotonation of **3** and formation of numerous species interconverting with various rates in solution. Although the accurate structural assignment of each species could not be carried out, analysis of the temperature dependent line shape together with 2D correlation and exchange

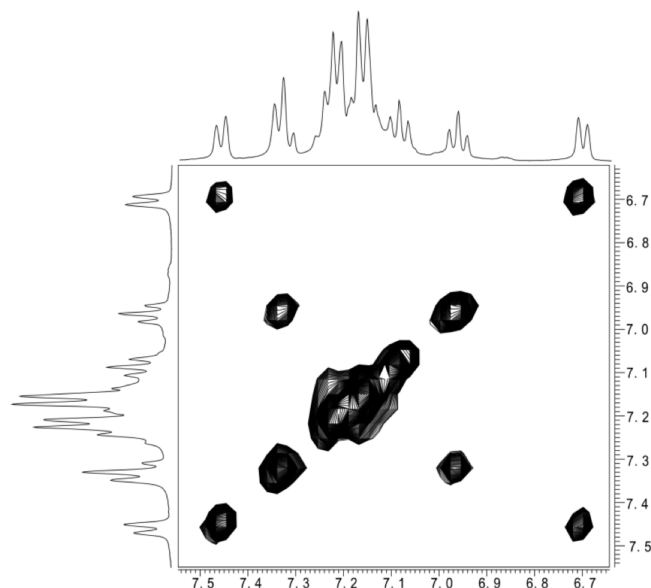
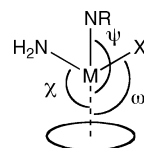


**Figure 2.** Section plot of phase sensitive 2D  $^1\text{H}$ - $^1\text{H}$  NOESY NMR spectrum (400 MHz,  $\text{CD}_2\text{Cl}_2$ ,  $-50\text{ }^\circ\text{C}$ ) of the sample obtained by addition of 1.5 equiv of dimethyl malonate **2** to a solution of amido complex **1a** in  $\text{CD}_2\text{Cl}_2$ . Only the cross-peaks corresponding to the chemical exchange are shown.

**Table 1.** Crystallographic Data for Complexes **6c** and **9c**

	<b>6c</b>	<b>9c</b>
empirical formula	$\text{C}_{35}\text{H}_{40}\text{N}_2\text{O}_6\text{SRu}$	$\text{C}_{35}\text{H}_{40}\text{N}_2\text{O}_6\text{SRu}$
formula weight	717.84	719.84
crystal color	colorless	colorless
crystal system	monoclinic	orthorhombic
space group	$P12_11$	$P2_12_12_1$
<i>a</i> , Å	8.098(2)	9.319(3)
<i>b</i> , Å	22.593(6)	14.771(4)
<i>c</i> , Å	17.761(5)	23.304(2)
$\alpha$ , deg	90	90
$\beta$ , deg	90.575(5)	90
$\gamma$ , deg	90	90
<i>V</i> , Å <sup>3</sup>	3249.4(15)	3207.5(14)
<i>Z</i>	4	4
absorp coeff, mm <sup>-1</sup>	0.595	0.599
reflections collected	13628	8888
independent reflections	11808	4987
refined parameters	891	397
<i>R</i> 1 ( <i>I</i> > 2 $\sigma$ ( <i>I</i> ))	0.0900	0.0860
$\chi$ , deg	129.11	129.92
$\psi$ , deg	131.19	133.53
$\omega$ , deg	125.96	130.11
bond length M-NH <sub>2</sub> , Å	2.129	2.141
bond length M-NR <sub>2</sub> , Å	2.180	2.103
bond length M-X, Å	2.221	2.095



- (12) C-enolates: (a) Bertani, R.; Castellani, C. B.; Crociani, B. *J. Organomet. Chem.* **1984**, 269, C15. (b) Wanat, R. A.; Collum, D. B. *Organometallics* **1986**, 5, 120. (c) Burkhardt, E. R.; Bergman, R. G.; Heathcock, C. H. *Organometallics* **1990**, 9, 30. (d) Suzuki, K.; Yamamoto, H. *Inorg. Chim. Acta* **1993**, 208, 225. (e) Veya, P.; Floriani, C.; Chiesi-Villa, A.; Rizzoli, C. *Organometallics* **1993**, 12, 4899. (f) Albeniz, A. C.; Catalina, N. M.; Espinet, P.; Redon, R. *Organometallics* **1999**, 18, 5571. (g) Tian, G.; Boyle, P. D.; Novak, B. M. *Organometallics* **2002**, 21, 1462. (h) Wolkowski, J. P.; Hartwig, J. F. *Angew. Chem., Int. Ed.* **2002**, 41, 4289. (i) Culkin, D. A.; Hartwig, J. F. *Organometallics* **2004**, 23, 3398.
- (13) Other C-bound complexes: (a) Ittel, S. D.; Tolman, C. A.; English, A. D.; Jesson, J. P. *J. Am. Chem. Soc.* **1978**, 100, 7577. (b) Crocco, G. L.; Lee, K. E.; Gladysz, J. A. *Organometallics* **1990**, 9, 2819. (c) Falvello, L. R.; Fernández, S.; Navarro, R.; Urriolabeitia, E. P. *Inorg. Chem.* **1997**, 36, 1136. (d) Kujime, M.; Hikichi, S.; Akita, M. *Organometallics* **2001**, 20, 4049. (e) Naota, T.; Tannna, A.; Kamuro, S.; Murahashi, S.-I. *J. Am. Chem. Soc.* **2002**, 124, 6482.

experiments carried out at  $-90\text{ }^\circ\text{C}$  and at  $-50\text{ }^\circ\text{C}$  allowed us to confirm the formation of O- and C-bound complexes as shown in Scheme 6.<sup>12-15</sup>

The Ru-CH protons of the interconverting C-bound complexes resonated in a narrow interval from  $\delta$  3.3 to  $\delta$  3.7; they overlapped with numerous signals of methoxy groups and CH protons and NH protons of the MsDPEN ligand. The CH protons of several interconverting isomers of the O-bound complex **9a** resonated as sharp singlets in the range from  $\delta$  4.2 to  $\delta$  5.0. Their origin could be easily verified by HMQC spectra by

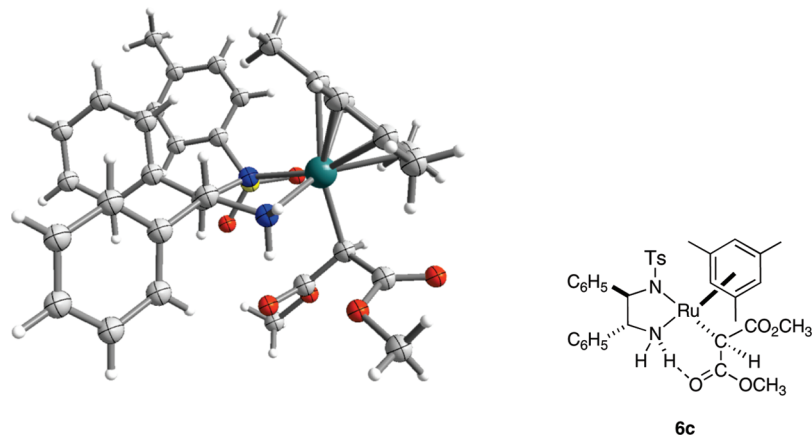
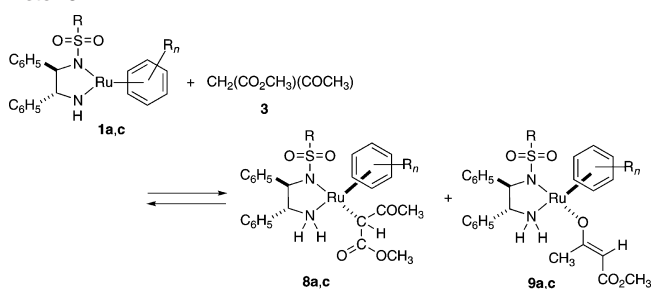


**Figure 3.** X-ray structure of complex **6c**.

**Scheme 6.** Reactions of Chiral Amido Ru Complexes with  $\beta$ -Keto Ester **3**



correlations with the carbon atoms with chemical shifts around  $\delta$  80–90 ppm (e.g., Figure 4). As shown in Figure 4, there are two major O-bound species not involved in the fast exchange at  $-50$  °C and several minor species including still broad signals.

Figure 5 shows the reversible line shape changes of the low-field part of the  $^{13}\text{C}$  NMR spectrum of the reaction mixture illustrating dynamic processes that take place in the system. At  $-90$  °C most of the dynamic processes are frozen, and there are roughly four signals of C-bound complexes (carbonyl groups at  $\delta$  168.2, 169.6, 169.7, 170.8 ppm) and four signals of O-bound complexes ( $\text{O}-\text{C}=\text{C}$  at  $\delta$  184.3, 184.5, 187.1, 188.5 ppm). The number of signals can be explained by taking into account the numerous possibilities of hydrogen bonding in the case of either **8a** or **9a** and conformations of the enolate fragment in **9a**. When the temperature was raised to  $-50$  °C, two signals at  $\delta$  169.6 and  $\delta$  169.7 were completely averaged, whereas the averaged signal at  $\delta$  185, which appeared from the exchange of the signals at  $\delta$  184.3, 184.5, and probably signals of other less concentrated species, was still broad; other signals changed their relative intensity. At  $25$  °C all signals in the carbonyl region including the signals of the excessive starting compound **3** were merged into the background due to the fast exchange between various C- and O-bound complexes, as well as between the amino and amido complexes.

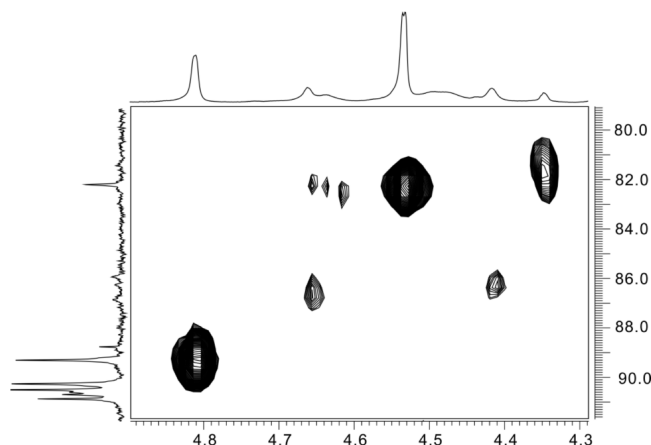


**Figure 4.** Section plot of HMQC  $^1\text{H}$ – $^{13}\text{C}$  NMR spectrum (400 MHz,  $\text{CD}_2\text{Cl}_2$ ,  $-50$  °C) of the sample obtained by addition of 1.5 equiv of  $\beta$ -keto ester **3** to a solution of amido complex **1a** in  $\text{CD}_2\text{Cl}_2$ . The relatively intensive signals at  $\delta$  89–90 in the  $^{13}\text{C}$  spectrum are from the coordinated  $\text{C}_6(\text{CH}_3)_6$  in various complexes.

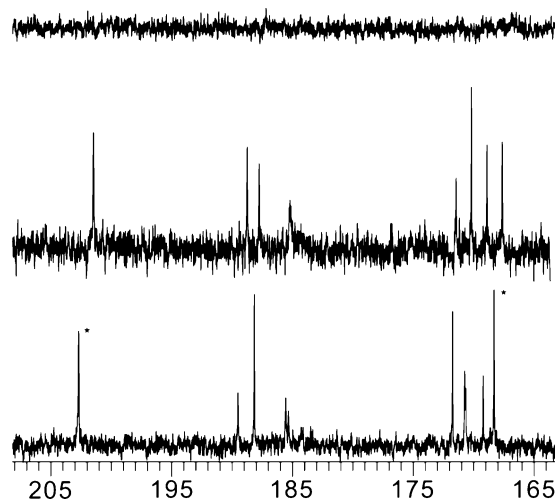


**Figure 5.** Section plots of the  $^{13}\text{C}$  NMR spectra (100 MHz,  $\text{CD}_2\text{Cl}_2$ ) of the sample obtained by addition of 1.5 equiv of  $\beta$ -keto ester **3** to a solution of amido Ru complex **1a** in  $\text{CD}_2\text{Cl}_2$ . Bottom: at  $-90$  °C (the signals of the excess starting compound **3** are marked with the asterisks); middle: at  $-50$  °C; top: at  $25$  °C.

The broadening of the spectral lines of **3** due to the exchange between the original and the deprotonated substrate in the  $^1\text{H}$  NMR spectrum became notable at  $-10$  °C. Hence, similarly to

- (14) O-eneolates: (a) Hagiwara, E.; Fujii, A.; Sodeoka, M. *J. Am. Chem. Soc.* **1998**, *120*, 2474. (b) Fujii, A.; Hagiwara, E.; Sodeoka, M. *J. Am. Chem. Soc.* **1999**, *121*, 5450. (c) Umebayashi, N.; Hamashima, Y.; Hashizume, D.; Sodeoka, M. *Angew. Chem., Int. Ed.* **2008**, *47*, 4196. (d) Sodeoka, M.; Hagiwara, E. *Chem. Commun.* **2009**, 5787. (e) Evans, D. A.; Mito, S.; Seidel, D. *J. Am. Chem. Soc.* **2007**, *129*, 11583. (f) Trost, B. M.; Xu, J.; Schmidt, T. *J. Am. Chem. Soc.* **2009**, *131*, 18343. (15) Equilibrium between C- and O-enolates: (a) Culkin, D. A.; Hartwig, J. F. *Acc. Chem. Res.* **2003**, *36*, 234. (b) Nishikata, T.; Yamamoto, Y.; Miyaura, N. *Organometallics* **2004**, *23*, 4317.

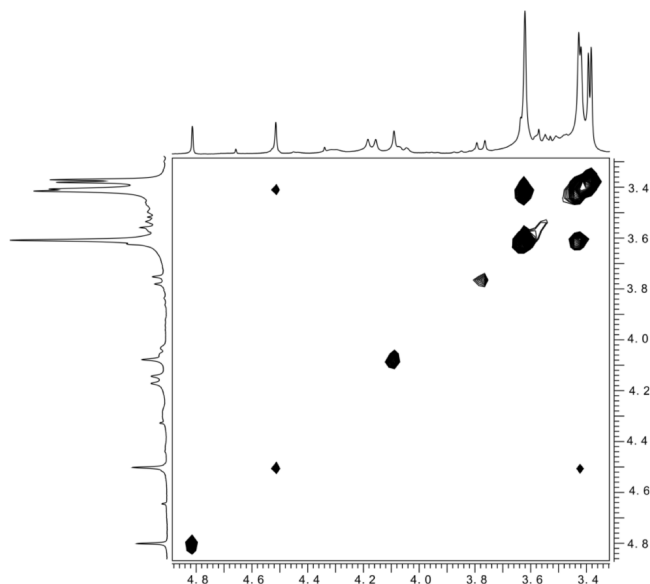


**Figure 6.** Section plot of phase sensitive 2D  $^1\text{H}$ – $^1\text{H}$  NMR NOESY spectrum (400 MHz,  $\text{CD}_2\text{Cl}_2$ ,  $-50^\circ\text{C}$ ) of the sample obtained by addition of 1.5 equiv of  $\beta$ -keto ester **3** to a solution of amido complex **1a** in  $\text{CD}_2\text{Cl}_2$ . The more intensive cross-peak corresponds to the exchange between two C-bound complexes, whereas the less intensive one attests for the exchange between O- and C-bound complexes that must occur directly, since the rate of deprotonation is too slow at this temperature.

the previous case, the deprotonation is notably slower than other dynamic processes in this system.

Interestingly, the phase sensitive 2D  $^1\text{H}$ – $^1\text{H}$  NOESY spectrum taken at  $-50^\circ\text{C}$  (Figure 6) showed that direct intramolecular interconversion (not involving the return to the amido complex) of the C- and O-bound complexes that do not have intramolecular H-bonds is possible. Indeed, analysis of the molecular structures suggested that in this case only slight intramolecular motion might be required to accomplish such a rearrangement as shown in Scheme 7. The computed difference in the stabilities of **8a** and **9a** is less than 1 kcal/mol (see further Table 3) which further supports our conclusion.

Very similar complicated equilibria between C- and O-bound complexes were observed for the reaction of amido complex **1c** with  $\beta$ -keto ester **3**. In the case of **1c** the structure of the O-bound complex **9c** was determined by single-crystal X-ray analysis (Table 1 and Figure 7).

Important structural features of complex **9c** are as follows: *S*-configuration of the Ru atom, *S*-*cis* conformation of the enolate

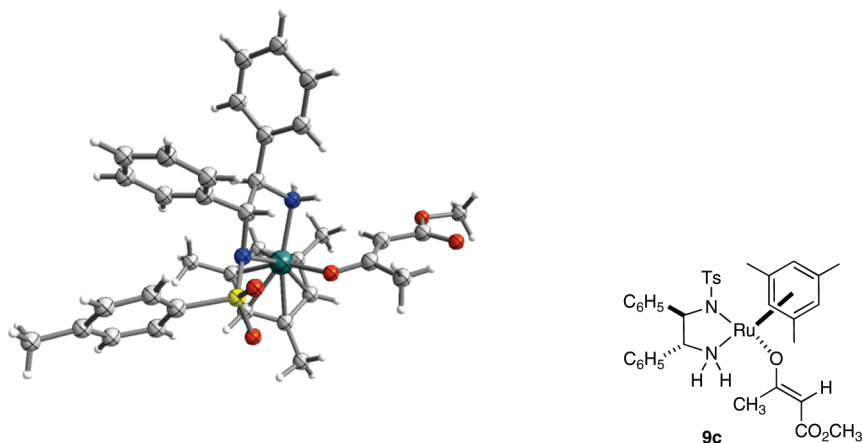
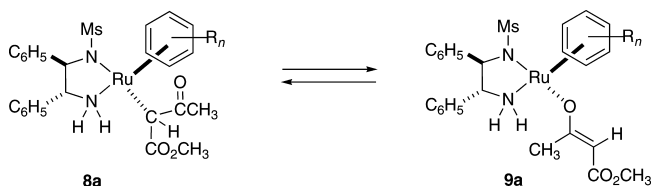


**Figure 7.** X-ray structure of complex **9c**.

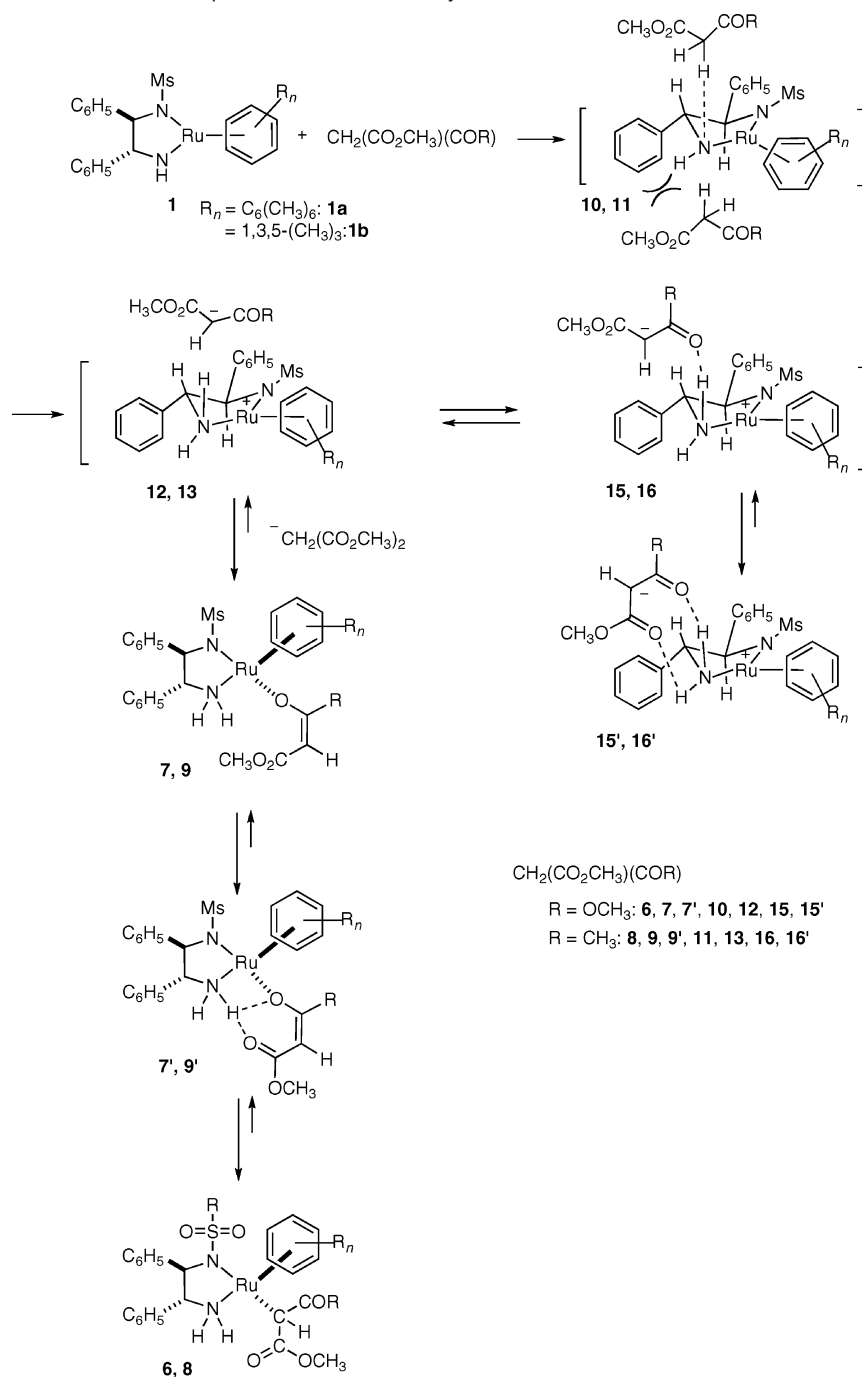
**Scheme 7.** Intramolecular Rearrangement between the C- and O-Bound Complex



coordinated to the metal, and significantly larger (for  $4^\circ$ ) angle made by the Ru–O bond and the plane of the coordinated arene compared to the angle made by the Ru–C bond in the C-bound complex **7c**. Most probably the O-bound complexes are kinetic products in the reaction of amido complexes with **2** or **3**; they can rearrange further into the C-bound compounds by simple intramolecular reaction as shown in Scheme 7.

**2.3. Computational Study of the Deprotonation Step.** In this work we were mostly interested in elucidating the mechanism of formation of the chiral environment (pocket) that results in the enantioselective reactions. Involvement of at least three molecules, the catalyst and two reactants, in the generation of a chiral product and an apparently multistage catalytic cycle makes this analysis nontrivial and challenging. There are several recent computational studies of the organocatalyzed asymmetric Michael addition of nitroalkenes<sup>16</sup> and  $\alpha,\beta$ -unsaturated imides.<sup>17</sup> However, we are unaware of any studies of the origin of enantioselection in the asymmetric Michael addition involving cyclic enones. It was important to use the real catalysts in the computations, since it is known that even slight simplification of the catalyst structure can result in a significant loss of the enantioselectivity.

At first we considered the possible mechanisms of the addition of cyclopentenone to the experimentally observed C- and O-bound complexes as shown in Scheme 8. It is quite clear that the proton transfer can take place only from one side of the chelate cycle of the Ru amido complex (e.g., **1b**, Scheme 8), since on the other side of the cycle the adjacent phenyl substituent effectively blocks the formation of dipole–dipole complexes with malonic ester, **10**, or  $\beta$ -keto ester, **11**. We have located transition states for the stereoselective proton transfer from **2** and **3** to the amido complexes **1a**–**c**. Table 2 lists computational data on the deprotonation step of **2** and **3** with the amido Ru complexes. The computed activation barriers for the proton transfer stage (14.7–16.0 kcal  $\text{mol}^{-1}$  in the case of **2** and 7.8–12.3 kcal  $\text{mol}^{-1}$  in the case of **3**) are in agreement with the NMR results confirming the rapid amido–amino

**Scheme 8.** Reactions of Chiral Amido Ru Complexes with 1,3-Dicarbonyls, **2** or **3**

equilibrium at ambient temperature. The uniformly higher values of the activation barriers in the case of **2** compared to those for **3** correspond to the higher Brønsted acidity of the latter compound.

The formation of ion pairs **12**, which are direct products of the stereoselective proton transfer from malonates **2**, is notably

- (16) (a) Hamza, A.; Schubert, G.; Soós, T.; Pápai, I. *J. Am. Chem. Soc.* **2006**, *128*, 13151. (b) Palomo, C.; Vera, S.; Mielgo, A.; Gómez-Bengoa, E. *Angew. Chem., Int. Ed.* **2006**, *45*, 5984. (c) Armó, M.; Zaragoza, R. J.; Domingo, L. R. *Tetrahedron: Asymmetry* **2007**, *18*, 157. (d) Yalalov, D.; Tsogoeva, S. B.; Schmatz, S. *Adv. Synth. Catal.* **2006**, *348*, 826. (e) Li, B.-L.; Wang, Y.-F.; Luo, S.-P.; Zhong, A.-G.; Li, Z.-B.; Du, X.-H.; Xu, D.-Q. *Eur. J. Org. Chem.* **2010**, 656. (f) Lu, D.; Gong, Y.; Wang, W. *Adv. Synth. Catal.* **2010**, 352, 644.
- (17) (a) Seebach, D.; Grošelj, U.; Badine, D. M.; Schweizer, W. B.; Beck, A. K. *Helv. Chim. Acta* **2008**, *91*, 1999. (b) Zhang, D.; Wang, G.; Zhu, R. *Tetrahedron: Asymmetry* **2008**, *19*, 568.

endothermic based on the positive  $\Delta E^1$  values as listed in Table 2, but they are quite stable to dissociation (Table 2,  $\Delta E^2$ ). The equilibrium can be shifted toward the amino Ru complexes via the intermolecular  $\text{S}_{\text{N}}2$ -type reaction<sup>10</sup> with another molecule of **2** (or its anion) that yields stereoselectively C- or O-bound complexes **6**, **7** (Table 3,  $\Delta E^3$ ). Another way of stabilization of the ion pairs **12** is via formation of the double H-bonds between the oppositely charged particles resulting in the formation of the ion pairs **15** as can be seen from the negative  $\Delta E^4$  values in Table 3.

We have optimized the geometries of the possible C- and O-bound complexes, **6**, **7**, and the H-bond stabilized ion pairs **15** to compare their relative thermodynamic stabilities (Table 3). One can see from Table 3 that although the ion pairs with a single hydrogen bond **15** are not stabilized compared to the

**Table 2.** Computational Data on the Deprotonation Step

$\text{Nu}^- = \text{CH}(\text{CO}_2\text{CH}_3)_2: \quad \mathbf{10}, \mathbf{12}$   
 $= \text{CH}(\text{CO}_2\text{CH}_3)(\text{COCH}_3): \quad \mathbf{11}, \mathbf{13}$

amido complex	Nu-H	TS	ion pair	$E_A^1$ , kcal mol <sup>-1</sup>	im. freq., cm <sup>-1</sup>	$\Delta E^1$ , kcal mol <sup>-1</sup>	$\Delta E^2$ , kcal mol <sup>-1</sup>
<b>1a</b>	<b>2</b>	<b>TS1</b>	<b>12a</b>	16.0	<i>i</i> 1225.7	15.4	78.7
<b>1a</b>	<b>3</b>	<b>TS2</b>	<b>15a<sup>a</sup></b>	9.7	<i>i</i> 1270.9	0.5	93.4
<b>1b</b>	<b>2</b>	<b>TS3</b>	<b>12b</b>	15.9	<i>i</i> 1251.8	14.4	82.9
<b>1b</b>	<b>3</b>	<b>TS4</b>	<b>13b</b>	12.3	<i>i</i> 1281.9	9.8	87.4
<b>1c</b>	<b>2</b>	<b>TS5</b>	<b>12c</b>	14.7	<i>i</i> 1267.8	13.3	81.3
<b>1c</b>	<b>3</b>	<b>TS6</b>	<b>13c</b>	7.8	<i>i</i> 1288.8	5.5	86.2

<sup>a</sup> In this case the corresponding ion pair **13a** could not be located, the optimization attempts invariably resulted in H-bound ion pair **15a**.

direct deprotonation products **12**, the relative stabilities of the chelating ion pairs **15'** are comparable to those of the corresponding C- or O-bound complexes, and they must be considered as kinetically available under the reaction conditions. The double H-bond stabilization effects on the reacting substrates are frequently observed in catalytic and enzymatic systems.<sup>18</sup>

Similar results were obtained for the deprotonation of  $\beta$ -keto ester **3** leading to the ion pairs **16** and the chelating ion pairs **16'** (Table 3). The computations correctly predict the higher stability of the C-bound complexes in the case of malonic ester **2** compared to the  $\beta$ -keto ester **3** and agree qualitatively with the experimentally observed equilibration between C- and O-bound complexes in the case of **3**.

**2.4. Origin of Enantioselectivity in the Michael Addition Reactions Catalyzed by Ruthenium Complexes.** We were initially impressed by the 3D-cavity suitable for accommodating a cyclopentenone molecule seen in the O-bound complexes (e.g., see the X-ray structure of **6c**) and accordingly tried to find the corresponding enantioselective reaction pathways. Thus, Figure 8 (top) shows the transition states **TS7-S** and **TS7-R** located by using the chiral pocket seen in the X-ray structure. The **TS7-S** is 2.9 kcal mol<sup>-1</sup> more stable than **TS7-R** that corresponds to the experimentally observed formation of the *S*-enantiomer of the reaction product. However, the activation energy of this C-C bond formation was computed to be 25 kcal/mol, which is hardly conceivable for a catalytic reaction taking place at ambient temperature. Moreover, no stable intermediate is formed after the C-C bond formation step, and even the intramolecular proton transfer that requires an additional 4.8 kcal mol<sup>-1</sup> yields a very crowded and quite unstable intermediate that must dissociate to make the whole transformation exothermic.

We reasoned then that there can be other similar transition states of lower energy if the enolate would acquire conformation allowing hydrogen bonding between its oxygen atoms and the NH<sub>2</sub> protons. Indeed, we have located such transition states (**TS8** and **TS9**) for *S*- and *R*-manifolds (Figure 8 middle and bottom). The hydrogen bonding does indeed decrease the energies of the corresponding transition states, e.g. for 7.6 kcal/mol in the case of **TS9-S** compared to **TS7-S**; however this decrease is mostly due to the stabilization of the starting complex, and the activation energies were high in all studied cases (Figure 8).

We concluded from these data that the catalytic cycle does not involve the formation of the O-bound complex. Apparently, the coordination of the cyclopentenone molecule to the NH<sub>2</sub> protons does not result in its effective activation. This is also seen in the quite short C-C bond lengths of the forming bond in the transition states **TS7-S**–**TS9** (Figure 8): they are very late transition states meaning that the reagents do not actually see each other until they are brought together quite closely.

We were also unable to find any reasonable reaction pathway starting from C-bound complexes. As seen from both the X-ray data and NMR results, these complexes are strongly spatially congested around the metal bound carbon center. Moreover, by making a covalent bond between the positively charged ruthenium atom and anionic carbon the reactive centers are essentially eliminated. Hence, we concluded that the formation of the isolable C- and O-bound complexes observed in the reaction of the Ru amido complexes and proton donors **2** or **3** is a dead end, and another mechanism must be sought.

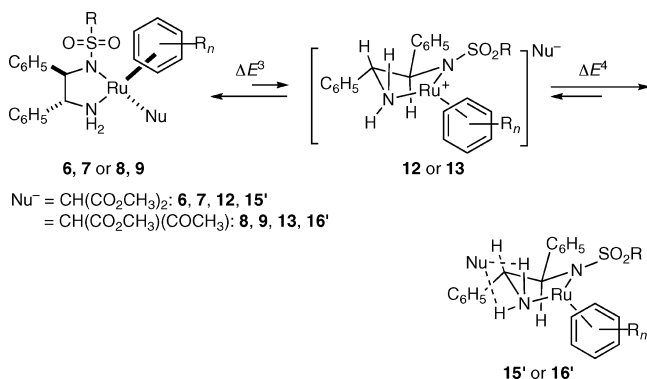
As discussed in Scheme 8, the chelating ion pairs **15'** must be kinetically available under the reaction conditions, since their stabilities are comparable to those of the C- and O-bound complexes. In addition, the H-bond stabilized nucleophiles are postulated as key intermediates in organocatalyst promoted C-C bond formation reactions.<sup>18a</sup> We reasoned, therefore, that a cyclopentenone molecule **4** can react with the chelating ion pairs **15'** or **16'** formed after the deprotonation of malonate **2** or  $\beta$ -keto ester **3**, respectively, as shown in Scheme 9. Due to the fast ring flipping in the ion pairs **15'** or **16'**,<sup>19</sup> the cyclopentenone molecule can approach either side of the chelate ring. In both cases *si*- and *re*-coordination of **4** is conceivable; hence there are four reactions to consider, two leading to the *S*-product, another two to the *R*-product. For the initial study we have chosen the reaction of  $\beta$ -keto ester **3** with cyclopentenone **4** catalyzed by the Ru complex **1b** that proceeds via the ion pair **16b'** to provide only moderate ee in order to be able to safely identify the pathway for the formation of the minor enantiomer.

As shown in Scheme 9, we have located stable zwitterionic complex **18b-S** with a positively charged Ru atom and the enolate anion coordinated by the NH<sub>2</sub> group. Moreover, starting

(18) (a) Takemoto, Y. *Org. Biomol. Chem.* **2005**, *3*, 4299. (b) Tsogoeva, S. B. *Eur. J. Org. Chem.* **2007**, 1701.

(19) We have studied the interconversion of **15'a(aa)** and **15'a(ee)** scanning the relative energy against the dihedral angle of the CHPh-CHPh unit. **15'a(aa)** is 2.9 kcal/mol more stable than **15'a(ee)**; the activation barrier converting **15'a(aa)** to **15'a(ee)** was estimated to be 3 kcal/mol.



**Table 3.** Computed Relative Energies (kcal/mol) of  $S_N2$  Type Reactions Converting Ion Pairs **12** or **13** to M–X Bound Complexes and Chelating Ion Pairs

$\text{Nu}^- = \text{CH}(\text{CO}_2\text{CH}_3)_2$ : **6, 7, 12, 15'**  
 $= \text{CH}(\text{CO}_2\text{CH}_3)(\text{COCH}_3)$ : **8, 9, 13, 16'**

Starting ion pair	amino complex	$\Delta E^\ddagger$		$\Delta E^\ddagger$ ion pair
		C-bound	O-bound	
<b>12a</b>	<b>6a</b>	-20.3		
	<b>7a</b>		-8.1 <sup>a</sup>	
	<b>7a'</b>		-18.8 <sup>b</sup>	
	<b>15a</b>			-3.2
	<b>15a'</b>			-18.3
<b>13a</b>	<b>8a</b>	-3.4		
	<b>9a</b>		-4.3 <sup>a</sup>	
	<b>9a'</b>		-12.6 <sup>b</sup>	
	<b>16a</b>			0.0
	<b>16a'</b>			-9.2
<b>12b</b>	<b>6b</b>	-22.7		
	<b>7b</b>		-5.3 <sup>a</sup>	
	<b>7b'</b>		-15.2 <sup>b</sup>	
	<b>15b</b>			-0.2
	<b>15b'</b>			-12.6
<b>13b</b>	<b>8b</b>	-16.7		
	<b>9b</b>		-13.0 <sup>a</sup>	
	<b>9b'</b>		-20.9 <sup>b</sup>	
	<b>16b</b>			-6.7
	<b>16b'</b>			-14.3
<b>12c</b>	<b>6c</b>	-21.8		
	<b>7c</b>		0.1 <sup>a</sup>	
	<b>7c'</b>		-10.8 <sup>b</sup>	
	<b>15c</b>			1.5
	<b>15c'</b>			-12.6
<b>13c</b>	<b>8c</b>	-15.8		
	<b>9c</b>		-12.5 <sup>a</sup>	
	<b>9c'</b>		-19.8 <sup>b</sup>	
	<b>16c</b>			-5.4
	<b>16c'</b>			-13.4

<sup>a</sup> *s-trans* conformation of the enolate (no HB). <sup>b</sup> *s-cis* conformation of the enolate (HB).

from **18b-S** we have found a transition state **TS10-S** for the mild C–C bond formation that was characterized by the activation barrier of only 8.6 kcal mol<sup>-1</sup> as depicted in Figure 9 and Scheme 10. The transition state **TS10-S** was 9.1 kcal mol<sup>-1</sup> lower in energy than **TS9-S**, the most stable transition state found for the alternative reaction pathway (Figure 8). Furthermore, it should be noted that the immediate product, **21b-S**, that is generated from ion pair **18b-S** through **TS10-S** is a stable intermediate having the structure of *O*-enolate bound to Ru. We investigated the possibility of the direct proton transfer in **21b-S** but could find only one with the activation barrier of 20.2 kcal mol<sup>-1</sup> (transition state **TSHC**). The barrier of the proton transfer to the oxygen atom was lower (16.9 kcal mol<sup>-1</sup>, transition state **TSHO**), and we have ascertained with the energy scan that the resulting enol complex **22b-S** can dissociate

without a notable activation barrier recovering the catalyst **1b** (Scheme 10). Under the real reaction conditions this stage is most probably strongly assisted by solvent as well as acidic donor substrates which directly protonate **22b-S** in an intermolecular manner, thus lowering the activation barrier.<sup>20</sup> Since it does not affect the stereoselectivity of the C–C bond formation, we did not attempt to study this process in more detail.

In order to access the reaction product with the opposite configuration, cyclopentenone can form either the intermediate **18b-R** or **20b-R** as shown in Scheme 9. The former is generated via coordination of the cyclopentenone molecule from the same side of the chelate cycle, but facing the enolate unit with the opposite prochiral plane. The intermediate **20b-R** is formed by coordination of the cyclopentenone molecule from the opposite side of the chelate ring. We have examined possibilities by locating both transition states **TS10-R** and **TS11-R**. As shown in Figure 10, in the **TS10-S** the steric hindrance is provided only from one side by the coordinated arene. This is enough, however, to effectively exclude the possibility of formation of **TS10-R**, since in that case the dimethylene unit of the cyclopentenone encounters the coordinated arene.

Due to the configurational flexibility of the Ru centers in the bifunctional Ru complexes,<sup>21</sup> the complex with the opposite configuration of the Ru atom is capable of arranging the cyclopentenone molecule via the favorable coordination mode that leads to the *R*-enantiomer via the transition state **TS11-R**. However, in this case one of the phenyl rings of the chelate cycle comes into play shielding the chiral box from another side as observed in Figure 10.

Computation revealed that the transition state **TS10-R** is by 8.1 kcal mol<sup>-1</sup> disfavored compared to the **TS10-S**, since in order to avoid the close contacts between the coordinated arene and the dimethylene bridge of the cyclopentenone one hydrogen bond must be broken. Hence, this pathway can hardly be expected to contribute into the formation of an *R*-product. On the other hand, the corresponding transition state **TS11-R** appeared to be only 1.8 kcal mol<sup>-1</sup> less stable than **TS10-S** due to the interaction of the cyclopentenone dimethylene bridge with the phenyl ring absent in the latter.

Similar transition states **TS10-S** and **TS11-R** have been located for a series of combinations of the catalyst and malonate or  $\beta$ -keto ester. Table 4 lists the representative computed data for these reactions. The activation energies were also computed in all studied cases and were in the range 3.4–6.7 kcal mol<sup>-1</sup> for the reactions of malonic ester **3** and in the range 6.4–10.4 kcal mol<sup>-1</sup> in the case of  $\beta$ -keto ester **4**.

In all studied cases the experimentally observed sense of enantioselection was reproduced via the proper sign of the difference in the ZPPE corrected computed energies or Gibbs free energies of the corresponding transition states. Moreover, qualitatively our computations reproduced the experimentally detected regular increase of the optical yield with the increasing bulk of the coordinated arene (Table 5).<sup>2d</sup> This trend can be explained by a stronger interaction of the coordinated cyclopentenone and the MsN–CH(C<sub>6</sub>H<sub>5</sub>) group in the transition state **TS11-R** with a bulkier coordinated arene.

(20) Handgraaf, J.-W.; Reek, J. N. H.; Meijer, E. J. *J. Am. Chem. Soc.* **2007**, *129*, 3099.

(21) Ito, M.; Osaku, A.; Kobayashi, C.; Shiibashi, A.; Ikariya, T. *Organometallics* **2009**, *28*, 390.

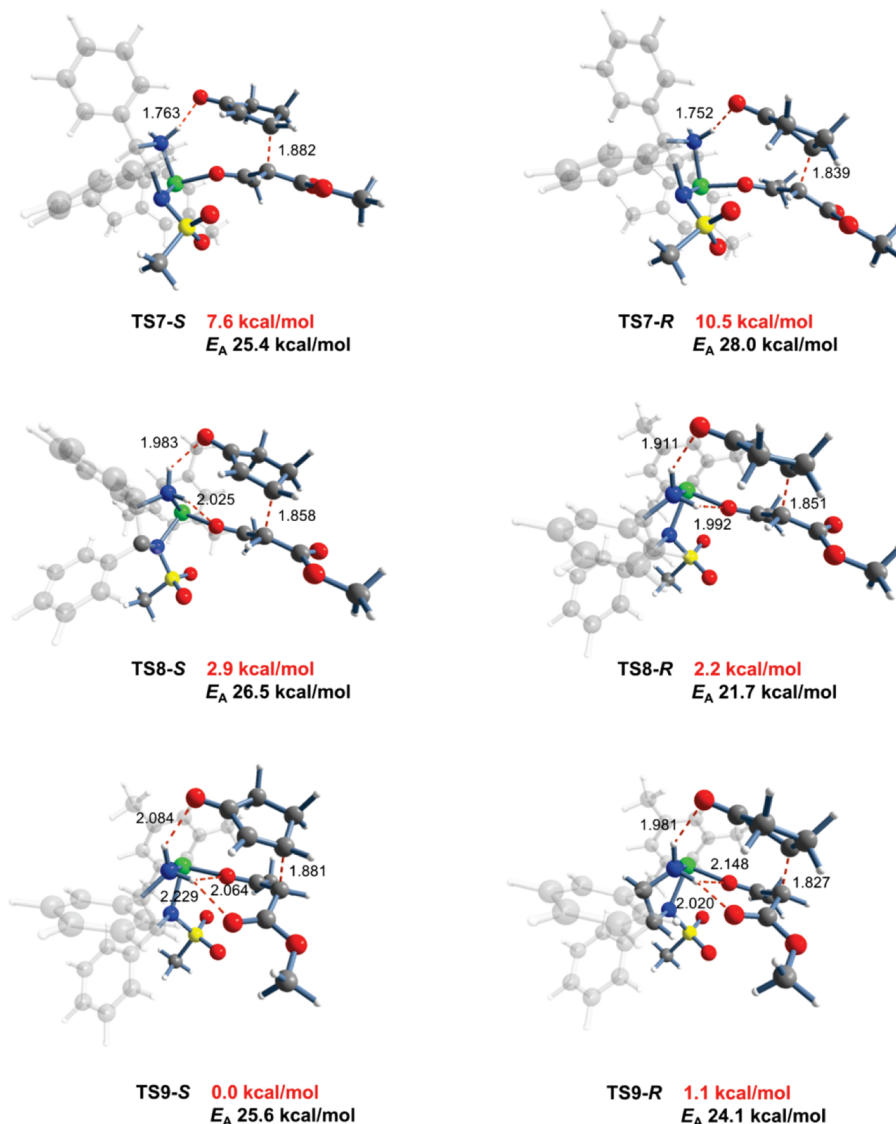


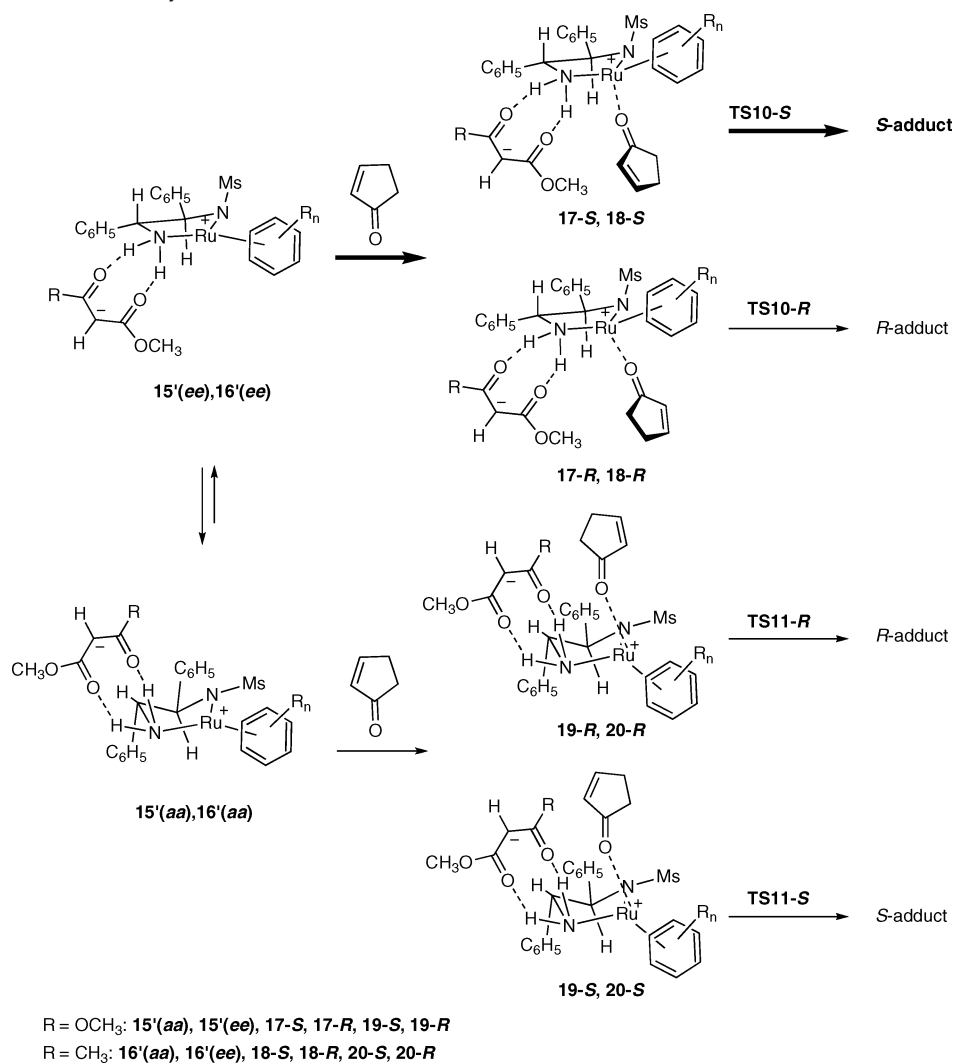
Figure 8. Structures and relative energies of the transition states TS7–TS9.

### 3. Conclusion

Our combined experimental and computational study of the enantioselective Michael addition of 1,3-dicarbonyls to cyclic enones with bifunctional chiral amido Ru complexes revealed that the reaction proceeds via the  $S_N2$ -type deprotonation of the donor molecule with the amido complex to the ion pair intermediate followed by enantioselective C–C bond formation. The stoichiometric reactions of the Michael donors, dimethyl malonates, or  $\beta$ -keto esters with bifunctional chiral amido Ru complexes showed that the deprotonation readily occurs at ambient temperature resulting in the equilibrium mixture that contains the starting amido Ru complexes and C- or O-bound Ru amino complexes. The reaction of malonic ester as the Michael donor gave the C-bound enolate complexes which were confirmed at low temperatures by the NMR data and by the single crystal X-ray analysis. In the reactions of  $\beta$ -keto esters with amido Ru complexes we have observed a formation of the complex mixtures of rapidly interconverting species, among which the O-bound enolates were reliably identified through their characteristic NMR features. This conclusion could be further confirmed by the X-ray structure of the O-bound enolate.

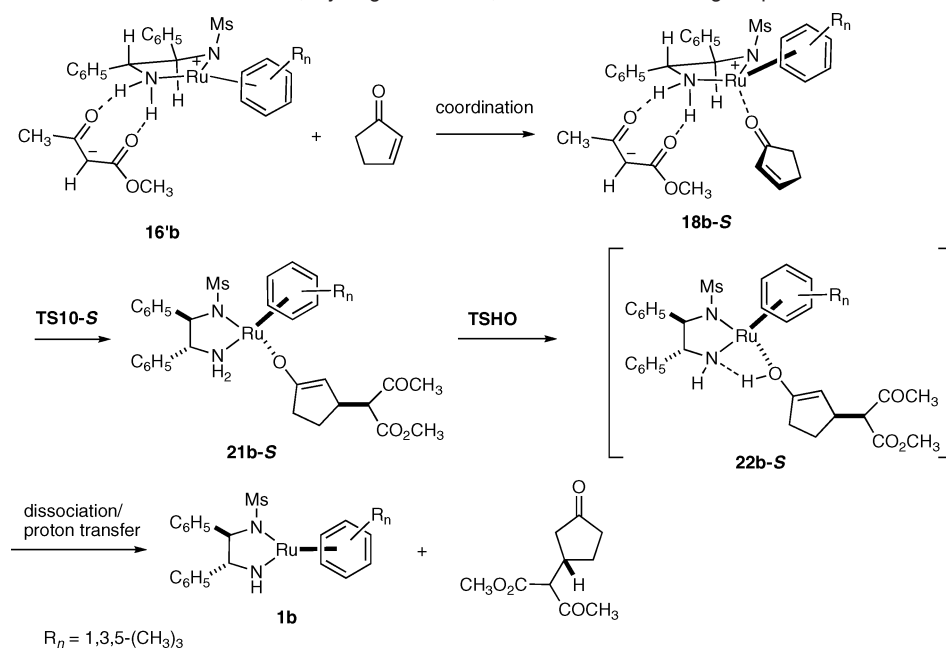
An initial computational analysis of the possible reaction pathways for the enantioselective C–C bond formation gave clear reasons to believe that neither of the experimentally characterized species is actually a reactive intermediate in this transformation. Several pathways computed for the reaction of the O-bound enolate complexes with cyclopentenone were characterized by activation energies of around 25 kcal/mol that is much higher than the expected activation barrier for catalytic reactions taking place at ambient temperature. The C-bound enolate complexes are too crowded and unreactive to accommodate a molecule of the cyclic enone in the coordination sphere for the enantioselective C–C bond formation.

Nevertheless, the computational studies revealed another possible mechanism of C–C bond formation that is characterized by notably lower activation barriers. If the enolate anion formed after the deprotonation of the donor molecules, instead of making a covalent bond with the positively charged Ru atom, forms a chelating ion pair with two amino protons, the metal center retains enough activity to coordinate a molecule of cyclic enone, and the enantioselective C–C bond formation proceeds through a tight-fitting assembly of the acceptor molecule and chiral ion paired complex. DFT analysis indicates that the ion

**Scheme 9.** Possible Reaction Pathways for Enantioselective C–C Bond Formation

pair intermediate is reasonably thermodynamically stable compared to other possible intermediates, C- and O-bound enolate

complexes. The key intermediate is the chelating ion paired complex formed by two strong hydrogen bonds of the  $\text{NH}_2$

**Scheme 10.** Enantioselective C–C Bond Formation, Hydrogen Transfer, and Product Releasing Steps

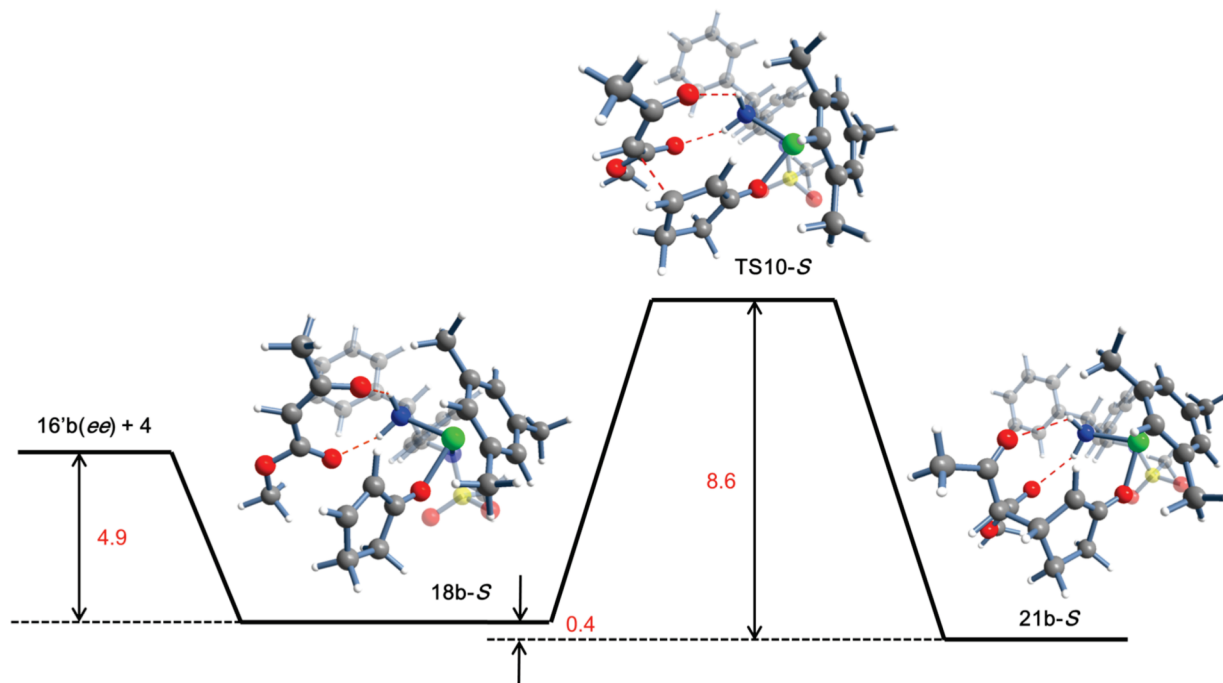


Figure 9. Profile of potential energy for the enantioselective C–C bond formation step.

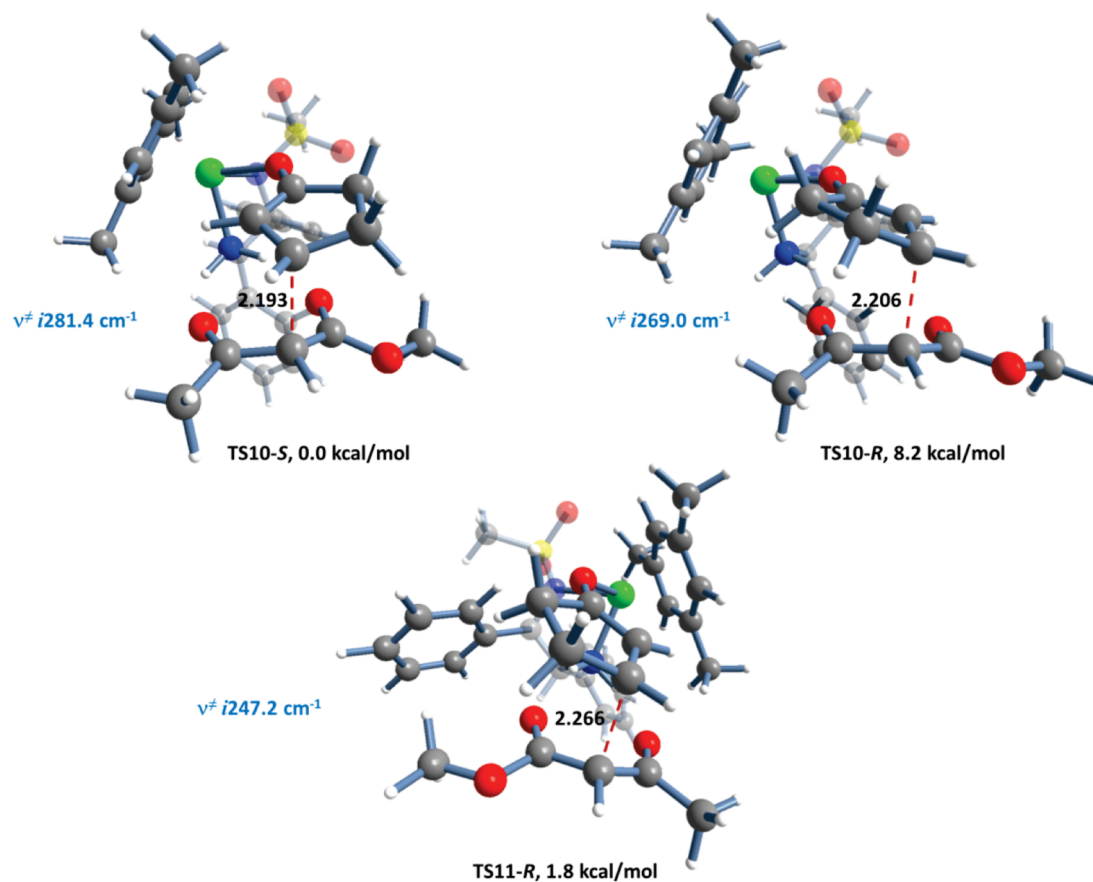


Figure 10. Optimized geometries and relative energies of the transition states **TS10-S**, **TS10-R**, and **TS11-R**. The **TS10-R** is strongly disfavored compared to the **TS10-S** due to the necessity to avoid close contacts between the dimethylene bridge of the cyclopentenone, the coordinating arene, and the alkyl substituent of the  $\beta$ -keto ester. In **TS11-R** the dimethylene bridge of the cyclopentenone is pointed apart from the coordinated arene, similar to the case for **TS10-S**. However, it approaches one of the phenyl groups in the chelate cycle, a close contact that is absolutely absent in **TS10-S** and **TS10-R**. The corresponding transition state for the formation of *S*-product (**TS11-S**) was not sought in this case, since it is expected to be still less stable than **TS10-R**.

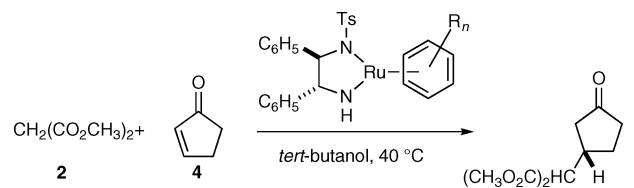
group that is capable of accommodating the molecule of electrophile yielding a ternary complex in which both substrates

are activated simultaneously. Thus, the bifunctional character of the Ru catalyst is fully exploited in creating a unique 3D

**Table 4.** Difference in Energies (ZPE Corrected) and Free Energies of the Computed Transition States for the Formation of *S*- and *R*-Products

Substrate	Sulfonyl group of the catalyst	Coordinated arene of the catalyst	$E_{\text{TS11-R}} - E_{\text{TS10-S}}$ kcal mol <sup>-1</sup>	$G(298)_{\text{TS8-R}} - G(298)_{\text{TS7-S}}$ kcal mol <sup>-1</sup>
Malonate	Ms	Hexamethylbenzene	4.7	6.3
		Pentamethylbenzene	3.7	5.3
		Mesitylene	1.7	2.6
		<i>p</i> -Cymene	0.3	1.8
	Ts	Hexamethylbenzene	3.7	5.1
		Pentamethylbenzene	2.6	4.0
		Mesitylene	1.1	3.0
		<i>p</i> -Cymene	0.6	1.8
$\beta$ -Keto ester <sup>a</sup>	Ms	Hexamethylbenzene	4.3	5.8
		Pentamethylbenzene	4.0	6.7
		Mesitylene	1.8	3.6
		<i>p</i> -Cymene	0.8	2.0
	Ts	Hexamethylbenzene	3.4	5.0
		Pentamethylbenzene	2.5	3.6
		Mesitylene	0.6	2.2
		<i>p</i> -Cymene	0.8	2.0

<sup>a</sup> In the case of  $\beta$ -keto ester the difference between slightly more stable transition states with the acetyl group oriented toward the coordinated arene is shown. Another couple of the transition states **TS10-S** and **TS11-R** was also computed for each case demonstrating the same tendency.

**Table 5.** Effect of Arene Ligand on Outcome of Asymmetric Michael Addition<sup>2d</sup>


Arene	Yield, %	ee, %	Difference of the free energies of the <i>R</i> - and <i>S</i> - pathways computed from the ee values
Hexamethylbenzene	98	98	2.3
Pentamethylbenzene	99	97	2.1
Mesitylene	99	89	1.2
<i>p</i> -Cymene	87	82	0.9

asymmetric environment that regulates the enantioselectivity of the catalytic reaction. A very similar mechanism of simultaneous substrate activation was recently outlined in the computational study of the Michael addition of acetylacetone to a nitro alkene catalyzed by chiral thiourea.<sup>16a</sup>

We are convinced that the present study of the mechanism of enantioselection in asymmetric C–C bond formation reactions with bifunctional Ru catalysts outlined important requirements necessary for the design of highly enantioselective transformations. Further studies along these guidelines are underway in our laboratories.

#### 4. Experimental Section

**General.** All NMR experiments were carried out in the JEOL ESX-400 instrument equipped with the field-gradient probe. Assignments of the signals in the spectra were carried out with the use of routine 2D correlation techniques.

**Complex 6a.** <sup>1</sup>H NMR (400 MHz, CD<sub>2</sub>Cl<sub>2</sub>, 223 K)  $\delta$ : 1.79 br. s (3H, CH<sub>3</sub> of mesyl), 1.98 s (18H, 6CH<sub>3</sub>), 3.34 br. m (4H, OCH<sub>3</sub>, NH), 3.49 s (3H, OCH<sub>3</sub>), 3.80 br. m (1H, CHPh), 3.95 br. s (1H, CH–Ru), 4.08 d (1H, CHPh), 6.45 br. m (1H, NH), 6.69 d (1H, *ortho*), 6.96 t (1H, *meta*), 7.09 t (1H, *para*), 7.32 t (1H, *meta*), 7.45 d (1H, *ortho*), 7.0–7.3 m (5H, C<sub>6</sub>H<sub>5</sub>); <sup>13</sup>C NMR (100 MHz, CD<sub>2</sub>Cl<sub>2</sub>, 223 K)  $\delta$ : 14.72 (6 Me), 27.04 (CH–Ru), 40.32 (OCH<sub>3</sub>), 43.87 (CH<sub>3</sub> of mesyl), 52.82 (OCH<sub>3</sub>), 66.11 (CHPh), 70.41 (CHPh),

90.72 (6C of hmb), 123.57 (br., CH *ortho*), 125.95 (br., CH *meta*), 126.74 (br., CH *para*), 127.21 (CH *meta*), 130.92 (CH *ortho*), 138.61 (C *tert*), 144.13 (C *tert*), 126.24, 126.44, 127.88 (5CH of another phenyl), 176.16 (C=O), 181.84 (C=O).

**Complex 6c.** <sup>1</sup>H NMR (400 MHz, CD<sub>2</sub>Cl<sub>2</sub>, 298 K)  $\delta$ : 2.07 s (9H, 3CH<sub>3</sub>), 2.25 s (3H, CH<sub>3</sub>), 3.70 br. m (7H, OCH<sub>3</sub>, NH), 3.87 br. m (1H, CHPh), 4.15 br. s (1H, CH–Ru), 4.31 d (1H, CHPh), 5.0 s (3H, mesitylene), 6.68 br. m (1H, NH), 6.6–7.5 m (14H, aromatic); <sup>13</sup>C NMR (100 MHz, CD<sub>2</sub>Cl<sub>2</sub>, 298 K)  $\delta$ : 18.03 (3 CH<sub>3</sub>), 18.63 (CH<sub>3</sub>, tosyl), 28.82 (CH–Ru), 50.49 (OCH<sub>3</sub>), 51.60 (OCH<sub>3</sub>), 67.97 (CHPh), 75.46 (CHPh), 85.67 (3CH of mesitylene), 94.19 (3C of mesitylene), 126.12, 126.66, 127.07, 127.24, 127.49, 127.62, 127.88, 128.09, 128.29, 128.43 (aromatic CH), 138.88, 139.63, 139.94, 140.44, 141.74, 144.61 (aromatic C), 178.04 (C=O), 181.93 (C=O).

**Computational Details.** All computations were carried out using the hybrid Becke functional (B3)<sup>22</sup> for electron exchange and the correlation functional of Lee, Yang, and Parr (LYP),<sup>23</sup> as implemented in the GAUSSIAN 09 software package.<sup>24</sup> For ruthenium, the SDD basis set with the associated effective core potential was employed.<sup>25</sup> All other atoms were modeled at the 6-31G(d) level of theory.<sup>26</sup> Test optimizations at several levels of theory for the compounds **6c** and **9c** with available X-ray structures were carried out for calibration purposes (see Supporting Information for details). It has been found that the introduction of the diffusion functions for the main group elements notably improves the reproducibility of the experimental bond lengths and valent angles within the B3LYP functional. The recently developed M052X functional<sup>27</sup> has been also tried. Since the results obtained with M052X/SDD(Ru)/6-31G\*(C,H,N,O,S) were almost identical with those obtained with B3LYP/SDD(Ru)/6-31G\*(C,H,N,O,S) (see Supporting Information for details), the latter functional has been chosen as the one most frequently used in the computational studies of

(22) (a) Becke, A. D. *J. Chem. Phys.* **1993**, *98*, 1372. (b) Becke, A. D. *J. Chem. Phys.* **1993**, *98*, 5648.

(23) Lee, C.; Yang, W.; Parr, R. G. *Phys. Rev. B* **1988**, *37*, 785.

(24) Frisch, M. J.; et al. *Gaussian 09*, revision A.02; Gaussian, Inc.: Wallingford, CT, 2009.

(25) Andrae, D.; Haeussermann, U.; Dolg, M.; Stoll, H.; Preuss, H. *Theor. Chim. Acta* **1990**, *77*, 123.

(26) (a) Ditchfield, R.; Hehre, W. J.; Pople, J. A. *J. Chem. Phys.* **1971**, *54*, 724. (b) Hehre, W. J.; Ditchfield, R.; Pople, J. A. *J. Chem. Phys.* **1972**, *56*, 2257. (c) Hariharan, P. C.; Pople, J. A. *Theor. Chim. Acta* **1973**, *28*, 213. (d) Hariharan, P. C.; Pople, J. A. *Mol. Phys.* **1974**, *27*, 209. (e) Gordon, M. S. *Chem. Phys. Lett.* **1980**, *76*, 163.

(27) Zhao, Y.; Truhlar, D. G. *Acc. Chem. Res.* **2008**, *41*, 157.

the transition metal catalytic reactions. Geometry optimizations were performed without any symmetry constraints ( $C_1$  symmetry).

Starting geometries for the transition state search were located either by QST2 or QST3 procedures, or by the guess based on the structure of the previously found TS. The transition states were subsequently fully optimized as saddle points of first order, employing the Berny algorithm.<sup>28</sup> Frequency calculations were carried out to confirm the nature of the stationary points, yielding zero imaginary frequencies for all Ru complexes and one imaginary frequency for all transition states, which represented the vector for the C–C bond formation or for the proton transfer in all respective cases. Zero-point energy corrections were carried out for all computed energies. The solvent influence has been checked by several single-point CPCM-SCRF calculations for THF and EtOH (see Table S2 in the Supporting Information). The relative energies computed in the gas phase or either of the solvents were found to be almost the same; hence the solvent influence was further neglected, and all shown data correspond to the zero-point energy

corrected gas phase values, as has been suggested in a recent work for a similar catalytic reaction.<sup>16a</sup>

**Acknowledgment.** This work was supported by a Grant-in-Aid for Scientific Research (Priority Areas No. 18065007, “Chemistry of *Concerto* Catalysis” and (S) No. 22225004) from the Ministry of Education, Culture, Sports, Science and Technology, Japan.

**Supporting Information Available:** NMR spectra for the stoichiometric reaction of amido complexes with 1,3-dicarbonyls. Experimental bond lengths and angles from the X-ray analysis of complex **6c** compared with the computed data. Representative computational results using CPCM-SCRF model for THF. Computational results (B3LYP//SDD(Ru)/6-31G\*) and atomic Cartesian coordinates for all the structures optimized in the DFT calculations. Complete ref 24. This material is available free of charge via the Internet at <http://pubs.acs.org>.

(28) Peng, C. Y.; Schlegel, B. *Isr. J. Chem.* **1994**, *34*, 449.

JA107597W